Water sorption isotherms and hysteresis of cement paste at moderately high temperature, up to 80 °C

Jiayi Wang [a], Marcus H.N. Yio [b], Tingtao Zhou [c], Hong S. Wong [b], Colin T. Davie [a], Enrico Masoero [a,d,*]

[a] School of Engineering, Newcastle University, NE1 7RU, Newcastle upon Tyne, UK
[b] Centre for Infrastructure Materials, Department of Civil and Environmental Engineering, Imperial College London, South Kensington, SW7 2AZ, London, UK
[c] Department of Mechanical and Civil Engineering, California Institute of Technology, 1200 East California Boulevard, Pasadena, 91125, CA, USA
[d] School of Engineering, Cardiff University, Queens Building, The Parade, CF24 3AA, Cardiff, UK

ARTICLE INFO

ABSTRACT

The constitutive models of concrete often consider water desorption isotherms to be near-equilibrium and significantly affected by moderately high temperature, 40–80°C, typically through microstructural changes. However literature data suggest that adsorption, not desorption, is near-equilibrium and moderate temperatures do not cause microstructural changes. This work supports the latter theory, through dynamic vapor sorption experiments on cement paste at 20–80°C. Samples were pre-conditioned at 60% relative humidity and 20°C, and isotherms were measured for several humidity ranges and testing rates. The results, corroborated by classical DFT simulations, indicate that adsorption is near-equilibrium and mostly unaffected by temperature, whereas desorption is out-of-equilibrium due to the ink-bottle effect at high humidity, and interlayer water at low humidity. Starting from the second cycle, desorption at higher temperatures features a shift of the cavitation pressure and overall a smaller hysteresis. A conceptual model of pore-specific temperature-dependent hysteresis is proposed to qualitatively explain the results.

1. Introduction

The water sorption isotherm of cement pastes is a key constitutive parameter in hygro-thermo-chemo-mechanical models of concrete [1–4]. The isotherms link relative humidity RH (or partial pressure) with saturation degree, both of which determine the effective pressure that causes humidity-induced deformations [5]. The isotherms are also related to the size distribution of mesopores, with width between 2 and 50 nm, hence they are a proxy for microstructure and can be used to infer other structure-sensitive properties (*e.g.* moisture permeability) or to validate microstructural models of the paste [6,7].

The impact of moderately high temperatures (40 to 80 °C) on the isotherm is important for cementitious materials in the energy sector, *e.g.* in the nuclear, geothermal, or oil and gas industries. Similar temperatures can also be reached during early hydration of cement in massive pours, possibly affecting the quality of the concrete. The current models consider that moderately high temperatures cause large changes in the isotherm [2,8]. This is supported by experimental results on first desorption isotherms using desiccators, some of which are shown in Fig. 1. In these experiments, the initial configuration is saturated, hence irreversible deformations upon first drying should be

expected irrespective of the temperature [9–11]. In most experiments in the literature, results are obtained in quasi-isobaric conditions and isotherms are later constructed under the assumption that desorption is near-equilibrium, *i.e.* that the distribution of water in the pores is such that it minimizes the free energy of the system at that given temperature and humidity; this implies path-independence, hence no difference when reaching the thermodynamic state by varying the temperature at constant humidity, rather than vice versa. Fig. 1.a,b shows examples of isotherms constructed in this way. True isothermal conditions, with RH being varied at constant temperature, were maintained in Ishida et al. [12] (reproduced in Fig. 1.c) and Brue et al. [13]; they both also recorded a significant impact of temperature on first desorption.

The current models commonly consider that changes on desorption are due to microstructural changes caused by the increase in temperature [2,3,18–25]. This is conceptually akin to how other properties, *e.g.* transport, change as a result of temperature-induced microcracks [26,27]. Poyet and Charles [8] proposed an alternative explanation for the desorption isotherms, without invoking microstructural changes: they showed that the Clausius–Clapeyron equation already captures the trends in Fig. 1, as long as the isosteric heat of sorption is
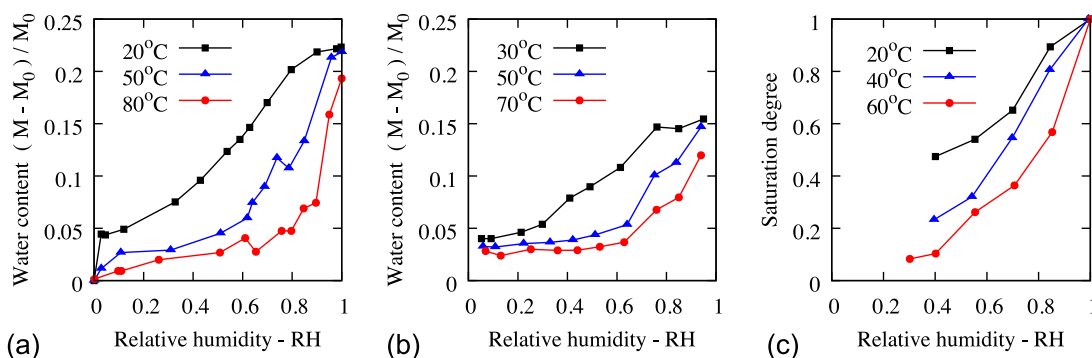

Fig. 1. First desorption isotherms at different temperatures on: (a) CEM I paste with water–cement ratio w/c = 0.4 from Drouet et al. [14], (b) CEM II paste with w/c = 0.3 from Abdelhamid et al. [15], (c) OPC paste with w/c = 0.5 from Ishida et al. [12]. Analogous results can be found in the work of Hundt and Kantelberg for mortar [16], of Poyet for high performance concrete [17], and of Drouet et al. for various types of cement pastes [14]. M and M_0 are respectively the sample mass at a generic RH and the dry mass after drying at 105 °C.
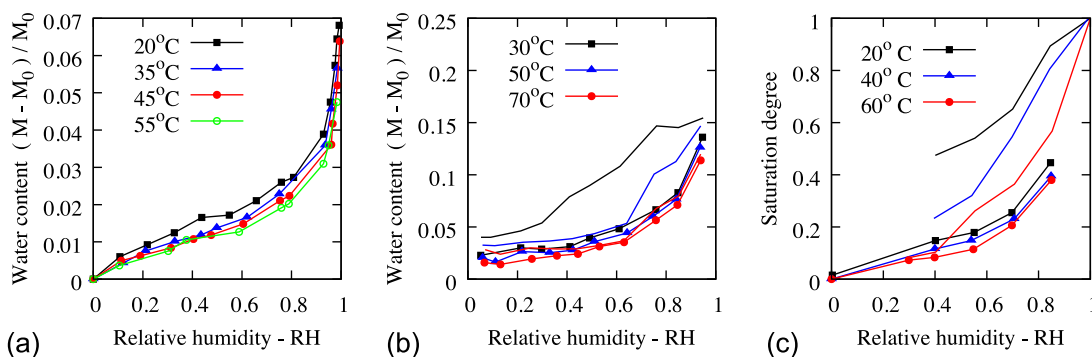

Fig. 2. Adsorption isotherms at different temperatures on: (a) mortar from Daian [28], (b) CEM II paste with w/c = 0.3 from Abdelhamid et al. [15], (c) OPC paste with w/c = 0.5 from Ishida et al. [12]. The dashed lines in (b) and (c) are the corresponding desorption branches from Fig. 1, to highlight their evolution towards adsorption as the temperature is increased.

properly fitted as a function of water content. Both these interpretations assume that the first desorption isotherm is near-equilibrium; otherwise, the resulting expressions should depend on kinetics. The validity of the near-equilibrium assumption, however, is questionable because: (i) results of first drying are significantly rate-dependent, whereas adsorption is much less so [10,12]; (ii) irreversible microstructural changes usually take place at the beginning of first desorption (at high RH) already in isothermal conditions [9–11]; (iii) experimental data on adsorption, shown in Fig. 2, are weakly dependent on temperature, whereas the desorption branches move towards the adsorption ones when temperature is increased (like an out-of-equilibrium state would move towards equilibrium [12]).

These observations suggest a different interpretation, where moderately high temperatures do not induce significant microstructural changes (except those that occur during first drying already in isothermal conditions, and that may depend on temperature), and where adsorption is near-equilibrium and desorption is out of equilibrium. This would be consistent with the trends in Fig. 2 and also with other observations from the literature, namely:

1. In the complex mesopore structure of cement pastes, hysteresis during sorption is controlled by the ink-bottle effect rather than by single-pore hysteresis, as confirmed by thermodynamic modeling and advanced simulations [5,12,29]. The ink-bottle effect moves desorption away from equilibrium, whereas the less important single-pore hysteresis would move adsorption out of equilibrium;
2. If one excludes microstructural changes, the current mathematical models of sorption would predict only small changes of equilibrium isotherms at moderately high temperatures, consistent with the adsorption isotherms in Fig. 2 [2,30];

3. Proton NMR (Nuclear Magnetic Resonance) experiments showed that temperature changes between 20 and 38 °C induced some structural changes, but these experiments only determined redistributions of water between interlayer and gel pores in calcium-silicate-hydrates (C–S–H), with negligible impact on the overall isotherm [31].

Furthermore, sorption isotherms from Dynamic Vapor Sorption (DVS) [32], reproduced in Fig. 3, feature adsorption branches that are similar to those in Fig. 2, supporting the interpretation that adsorption is near-equilibrium. By contrast, the desorption branches from DVS differ significantly from those obtained using the static gravimetric method with desiccators (*cf.* Fig. 3 with Fig. 1). In particular, desorption from DVS is weakly affected by temperature, except for an increase of the cavitation pressure, highlighted in Fig. 3, and less hysteresis especially at low RH below cavitation. The results in Fig. 3 refer to the second cycle of desorption and adsorption, excluding irreversible deformations from first drying (although the same work also reported small changes from first to second desorption, suggesting that microstructural changes during drying might be viscous and unable to fully develop in the shorter timescales of DVS experiments, compared to traditional experiments with desiccators). A limitation of the results in Fig. 3 is that they cover only a small range of temperature, from 25 to 40 °C.

In this article, we present new DVS results on cyclic sorption of CEM I paste at 20, 40 and 80 °C, in isothermal conditions. To reduce confounding effects from irreversible changes upon first drying at high RH and harsh drying, we pre-conditioned all the samples to RH = 60% and limited desorption to a minimum RH of 5%. The results confirm and extend those in Fig. 3, supporting the interpretation that adsorption is near-equilibrium and desorption is not. Desorption curves obtained at 80 °C follow the trend from Fig. 3, showing a further increase in
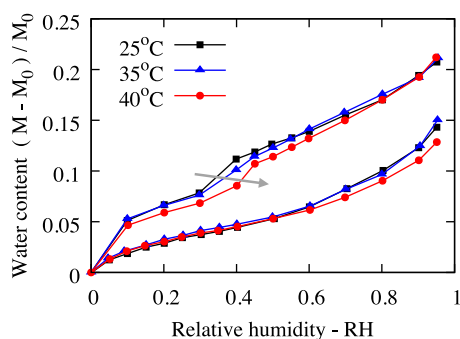
Fig. 3. Second-cycle sorption isotherms of CEM I pastes with w/c = 0.4 at different temperatures [32]. The arrow indicates the increase of cavitation pressure, *viz.* the RH at which the desorption curve drops due to rupture of capillary menisci.

Table 1
Composition and properties of CEMI 52.5R/85.

Quantity	Value	Units
CaO	65.7	%
SiO_2	21.6	%
Al_2O_3	4.05	%
SO_3	3.30	%
MgO	1.30	%
Fe_2O_3	0.26	%
K_2O	0.35	%
Na_2O	0.30	%
Chloride (Cl^-)	0.01	%
Free CaO	1.60	%
Loss on ignition	3.20	%
Specific weight	3.06	g/cm^3
Blaine surface area	4600	cm^2/g
Initial setting	100	min
Final setting	130	min

cavitation pressure and inducing a further reduction of the overall hysteresis. The shift of cavitation pressure is qualitatively confirmed by dedicated simulations using classical Density Functional Theory (DFT), which attribute the out-of-equilibrium state of desorption to the ink-bottle effect of water in gel and capillary pores. The article then explores how the temperature-dependent isotherms change when drying to nominal RH = 0%, instead of stopping at RH = 5%; this highlights the role played by interlayer water in the C–S–H. Additional experiments address the impact of the maximum RH reached during the sorption cycles (80% *vs.* 98%), the precision with which the mass of the samples is stabilized after changing RH (this controls the rate of the experiment), the differences between first and second sorption cycles, and the scope and limitations of normalizing water content by dry mass. Finally, a conceptual model is proposed for the temperature-dependent hysteresis from water in interlayer spaces and in larger pores (gel and capillary). The model offers a qualitative explanation for the experimental trends and a starting point for future, improved constitutive laws of temperature-dependent water sorption in cement pastes.

2. Methods

2.1. Materials and samples preparation

We consider samples of CEMI 52.5R/85 paste with water–cement ratio 0.4, whose isotherms have been already measured in the literature using both desiccators and DVS, as discussed in the introductory section. The chemical composition and key properties of the cement are summarized in Table 1.

The cement paste was prepared in the laboratory in a single batch, using deionized water and a paddle mixer, and manually tapped to

remove air bubbles. Eight cylindrical specimens with 15 mm diameter and 10 mm height were cast in total. The molded samples were wrapped in cling film and at 20 °C in an air-tight plastic box. The samples were demolded after 7 days of hydration and then put back unwrapped into the same box for further curing, along with a tray filled with deionized water to keep the RH at 100%, until 28 days. After that, the samples were moved to a new air-tight box, this time containing a tray filled with saturated aqueous solution of ammonium nitrate, to keep the RH inside the box to ~60%, while always at 20 °C [33–35].

The samples were kept at 60% RH for slightly over 6 months before starting the subsequent sorption tests. The initial RH of 60% was chosen for three reasons. First, to exhaust the large irreversible microstructural changes that occur at high RH during first desorption (*e.g.* coarsening of capillary and large gel pores), hence providing a more stable microstructure to start the tests with[1] Second, to stop further hydration, as hydration of alite, the principal phase in Portland cement, is known to stop when exposed to RH below 80% [36]. Third, to set the samples to a typical relative humidity for engineering applications; in this way we aimed for a realistic level of microstructural deformations, expected during first drying, while avoiding excessive deformations that drier conditions would cause, but also avoiding the unrealistic absence of such deformations and the continuing hydration that a higher RH would produce. One risk of pre-conditioning samples at 60% RH is that during the sorption tests, at RH > 80%, the samples may start hydrating again; this would change their microstructure and may complicate the interpretation of the results. However, our results (both for adsorption limited to 80% RH and exceeding it) will show that further hydration, if present at all, has a negligible impact on the isotherms, which turn out to be consistent between first and second sorption cycles.

In preparation for the water sorption tests, fragments were chiseled out from some of the samples, with masses M_i in the 35–200 mg range: see Table 2 (the DVS machines used in the work can test samples with mass up to 1 g). To check that the fragmentation did not induce significant microstructural changes at the isotherms-relevant scales (tens of nanometres), we exposed two of the original disks and four fragments to a range of RH (between 50% and 80% in steps of 10%) in a climate chamber at 20 °C (BINDER KBF 240), verifying that their relative weight changes were indeed comparable. This confirmed previous literature works, which already showed that extracting fragments from larger samples has negligible impact on the measured sorption isotherms and on the related mesopore structure [37,38]. The preliminary tests in climate chamber took approximately 5 months.

2.2. Sorption isotherms using DVS

The Dynamic Vapor Sorption (DVS) analyzers used in this work were the *DVS Intrinsic Plus*, which can go up to 40 °C and 98% RH, and the *DVS Resolution*, which also covers the 0%–98% range of RH up to 40 °C but can also reach 85 °C, although at this temperature its maximum RH is limited to 80%. Both analyzers are from *Surface Measurements Systems Ltd*. Both analyzers house a 6 digit microbalance for measuring sample weight change under controlled temperature and RH, in a nitrogen atmosphere. A more detailed description of the analyzer can be found in the literature [32,39]. One advantage of DVS is that measurements are carried out in true isothermal conditions, by controlling and varying directly the RH, instead of reconstructing isotherms from isobaric conditions in desiccators (see previous discussion of Fig. 1). Another advantage of DVS is that both RH and temperature are controlled with high precision ($\pm1\%$ RH, ±0.1 °C)

---

[1] Irreversible structural changes continue all the way down to 0% RH during first drying, but they are minimal during subsequent cycles [11]. Reversible structural changes persist during subsequent cycles, but they do not affect the shape of the isotherms as long as enough time is given for the sample to adapt after a humidity change.

Table 2

List of all the samples tested by DVS. ε is a threshold value of relative mass change used by the DVS machines to establish when a sample is sufficiently stable at any given RH. All samples were tested using either $\varepsilon = 10^{-5}$ or 10^{-6} min^{-1}. In various cases, different ε were used during the first and second sorption cycles: the values of ε will be specified case-by-case in the results section. The only exception is sample C2 at 80 °C, which was tested at a lower $\varepsilon = 3 \cdot 10^{-7}$ min^{-1} to evaluate rate effects in comparison with sample C1-80 °C, tested under the same protocol but with a larger, less restrictive ε. M_i is the sample mass after pre-conditioning at 60% RH, before starting the DVS tests. M_{10} is the sample mass at 10% RH during second-cycle adsorption. M_0 is the dry sample mass, after 24 h at 105 °C.

Sample ID and temperature	Sorption protocol description	M_i (mg)	M_{10} (mg)	M_0 (mg)
A-20 °C	5%–80% RH	40.672	39.000	36.100
B1-20 °C	5%–98% RH	191.432	181.516	176.510
B2-20 °C	5%–98% RH	41.151	39.654	36.800
C-20 °C	0%–98% RH	47.606	44.406	43.354
A-40 °C	5%–80% RH	40.878	38.773	36.400
B-40 °C	5%–98% RH	91.095	85.922[a]	82.510
C-40 °C	0%–98% RH	59.058	53.814	52.280
A-80 °C	5%–80% RH	36.525	32.987	32.100
C1-80 °C	0%–80% RH, $\varepsilon = 10^{-5}$ min^{-1}	37.242	34.183	33.322
C2-80 °C	0%–80% RH, $\varepsilon = 3 \cdot 10^{-7}$ min^{-1}	41.180	37.507	36.300

[a]This value of M_{10} refers to first-cycle adsorption, as second-cycle data were lost for this sample.

whereas such control can be more difficult to achieve with the conventional desiccator method. Furthermore, experimental programs can be set up in DVS to automatically run multiple cycles of adsorption and desorption without the need to remove the samples, differently from tests in desiccators where, often, samples are moved from one chamber to another, or the chamber is opened to replace salt solutions or to weigh the samples.

The DVS measurements in this work explore several ranges of RH at three different temperatures: 20 °C, 40 °C, and 80 °C. The tests at 20 and 40 °C were performed on the *DVS Intrinsic* apparatus, which controls RH between 0 and 98%. The tests at 80 °C were conducted on the *DVS Resolution* machine, which can control the RH between 0 and 85% when operating at 80 °C. All the tests started from the samples after the aforementioned pre-conditioning at 60% RH and 20 °C. After placing the samples into the DVS analyzer, the temperature was increased to 40 °C or 80 °C, as needed, while keeping the RH at 60%; this typically caused an initial decrease in water content, even when the temperature in the DVS was kept at 20 °C, despite the samples were pre-equilibrated for a long time already. Then the RH was reduced in steps of 10% until reaching RH$_{min}$ (5% or 0%, depending on the test), then increased in steps of 10% to reach RH$_{max}$ (80% or 98% depending on the test), then reduced again in steps of 10% back down to 60%, to complete the first sorption cycle. This was immediately followed by a second cycle with the same protocol.

DVS isotherms were obtained for a range of stabilization thresholds ε, which is a parameter that is set in the DVS apparatus software and defines the rate of relative mass change of a sample below which it is considered as stable, and the experiment moves to the next RH. The calculation of ε in the DVS apparatus changes with software version; the typical values used for DVS measurements of cement-based materials are in the order of 10^{-5} min^{-1} [32,39,40]. In this work, we used ε values of $3 \cdot 10^{-7}$, 10^{-6}, and a more generous 10^{-5} min^{-1}. In addition, we imposed that any RH level was to be maintained for a minimum of 6 h, and a maximum of 72 h. To provide a more precise interpretation of this ε threshold, for each step of RH we also computed a related quantity, ε_a, defined as follows:

$$\varepsilon_a = \frac{1}{\Delta t} \cdot \frac{M(t + \Delta t) - M(t)}{M(t)} \tag{1}$$

Δt is the averaging time, which we set to 10 min. From our experiments we found that our stabilization criteria above led to an average ε_a between $5 \cdot 10^{-6}$ and $7 \cdot 10^{-6}$ min^{-1} when using $\varepsilon = 10^{-5}$ min^{-1}, an

average ε_a between 10^{-7} and $7 \cdot 10^{-6}$ min^{-1} when using $\varepsilon = 10^{-6}$ min^{-1}, and an average ε_a between $8 \cdot 10^{-7}$ and $2 \cdot 10^{-6}$ min^{-1} when using $\varepsilon = 3 \cdot 10^{-7}$ min^{-1}. Fig. 4 shows typical mass plots obtained in this study. The figure shows that the samples attained a stable mass at all RHs except very low (from 10% down to 0%) and very high (90% to 98% RH at 20 °C and 40 °C, 70% to 80% at 80 °C) ones. Poor convergence to a stable mass was also recorded in proximity of the RH corresponding to cavitation during desorption, *i.e.* RH between 30% and 50%, but not during adsorption, which corroborates the view that adsorption is near-equilibrium. However, in general, the mass stabilization achieved was satisfactory to produce meaningful trends that will be discussed later in the result sections. Fig. 4 also highlights the timescale of the experiments at different temperatures, with tests conducted at 20 °C and 40 °C both requiring approximately 40 days to complete two full cycles of sorption, whereas comparable tests at 80 °C could be completed in just 4 days.

Here we normalize the water content of each sample by its mass at 10% RH during the second-cycle adsorption, M_{10}. In the literature, water contents are commonly normalized by dry mass M_0 instead. Here, however, we will stop some of our tests at RH$_{min} = 5\%$, at which point the evaporation of interlayer water will be only partial, and its extent will be most likely temperature-dependent. We will show how this, when normalization by M_0 is employed, leads to a situation where neither the adsorption nor the desorption branches at different temperatures are consistent. Instead, normalizing by a suitably low mass will allow us to exclude the impact of interlayer water motion when RH gets close to 0% [5,9,41–43]. The reason for choosing M_{10} on an adsorption branch, and not during desorption, is that our results support the thesis that adsorption is near equilibrium, hence using a mass on the adsorption branch is a more robust and repeatable choice. The reason for using M_{10} from the second-cycle adsorption is that normalization by M_{10} during first adsorption would produce less consistent isotherms.[2] This suggests that only when a full cycle of adsorption and desorption is completed, all the irreversible microstructural changes and other sources of hysteresis (e.g. motion of interlayer water) are exhausted, yielding stable samples that can produce repeatable isotherms (as long as the bounds of RH$_{min}$ and RH$_{max}$ used during the first cycle are respected).

To check consistency between results from different sorption apparatuses, Fig. 5 compares the second-cycle isotherms obtained at 20 °C using the *DVS Intrinsic Plus* and the *DVS resolution* analyzers. The isotherms indicate that the results were indeed comparable, both absolute values of adsorbed water and gradients at any RH. The only significant discrepancies between curves are at high RH, where a larger variance in the isotherms is expected due to the exponential relationship between the RH and the size of pores where water can condense (*e.g.* from the Kelvin equation). Other smaller quantitative differences do not affect the major qualitative changes in sorption curves observed at high temperatures, and reported later in this article. Therefore all measurements can be considered together despite being collected using two different analyzers.

2.3. Simulations of adsorption and desorption

We consider model configurations of the mesostructure of hydrated cement pastes (from nano to micro), which is represented as a packing of spherical nanoparticles, polydisperse in size, as presented in previous works [44,45]. Condensation and evaporation were simulated using a discrete lattice gas density functional theory (DFT) with interaction parameters imported from atomistic simulations of water in contact with cement minerals [41]. This DFT approach was first derived by

---

[2] Here we do not present data normalized by M_{10} during first adsorption, but the interested reader can reconstruct such normalized isotherms from the data in the figures and the values of second-adsorption M_{10} in Table 2.
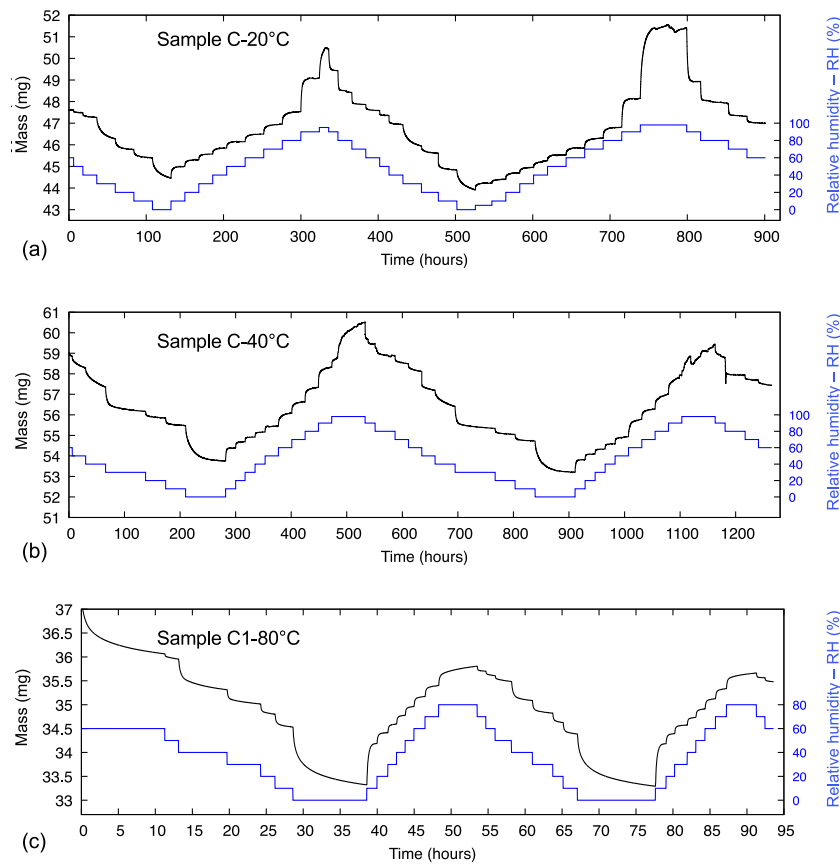
Fig. 4. Evolution of sample mass during DVS cycles of adsorption and desorption: (a) Sample C-20 °C tested with $\varepsilon = 10^{-6}$ min^{-1}; (b) Sample C-40 °C with $\varepsilon = 10^{-6}$ min^{-1}; (c) Sample C1-80 °C with $\varepsilon = 10^{-5}$ min^{-1}.
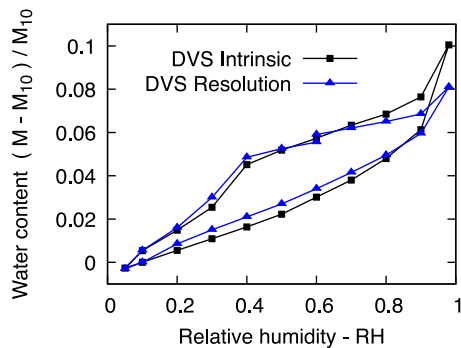

Fig. 5. Second-cycle isotherms of our sample (CEM I, w/c = 0.4) at 20 °C, run on the two apparatuses used in this work: *DVS Intrinsic* and *DVS Resolution*. For both curves, the stabilization threshold is $\varepsilon = 10^{-6}$ min^{-1}.

Kierlik et al. [46,47] for adsorption/desorption of a fluid in a quenched random porous solid. The method was previously applied to study the capillary stress and drying shrinkage of cement pastes [29,48].

The first step in the DFT simulations is to overlay a cubic lattice grid onto the particle-based configuration. If the center of any grid cell falls within the volume of a solid particle, the cell is marked as $\eta = 1$, otherwise it is treated as a pore where water can condense and evaporate, marked as $\eta = 0$. The interaction energy between a cell and its first neighbors is given by two parameters: w_{ff} if both neighboring cells are filled with fluid, w_{sf} if one cell is solid and the neighbor is filled with fluid. The chemical potential μ of the fluid to be adsorbed is fixed; in case of water sorption, this is linked to the partial pressure and thus the RH of the water vapor surrounding the sample. For any value

of μ, the corresponding amount of water condensing in each available site (with $\eta = 0$) is obtained by minimizing the grand potential:

$$\Omega = -w_{ff} \sum_{\langle i,j \rangle} \rho_i \rho_j - w_{sf} \sum_{i,j} \rho_i \eta_j - \mu \sum_i \rho_i + k_B T \sum_i \left[\rho_i \ln \rho_i + (1 - \rho_i) \ln(1 - \rho_i) \right] \tag{2}$$

where ρ_i, the normalized density of fluid on site i, can vary continuously between 0 and 1. Subscript j identifies the 6 first-neighbor cells of cell i. The fluid–fluid interaction energy w_{ff} is determined by the bulk critical point $k_B T_c = -v w_{ff}/2$ where $v = 6$ is the number of nearest neighbors in the cubic lattice. The lattice spacing a of the DFT simulations is estimated from the surface tension that is energy per area $\gamma \sim w_{ff}/2a^2$. For water at $T = 300$ K, $\gamma \sim 72$ mN/m which gives $a \sim 0.24$ nm. Based on these estimates, we choose a fine grid cell size of $a = 0.3$ nm i.e close to molecular size. The fluid-solid interaction energy $w_{sf} = 2.5 \ w_{ff}$ is estimated from molecular simulations of the isosteric heat of adsorption in the limit of zero coverage for water in cement paste [41].

With the presented method, the total water contents in the model configuration for sets of increasing/decreasing values of μ provide respectively the adsorption and desorption isotherms. In particular, here we will test the effect of temperature on the isotherms. As the temperature is increased from the room temperature value $T = 300$ K, the last (entropic) term of Eq. (2) becomes more significant, and the system is brought closer to its critical point T_c. This will lead to a reduction of the hysteresis between adsorption and desorption branches, and indeed one expects that hysteresis should disappear at and above T_c.

3. Results

The main results of this study are second-cycle DVS isotherms between 20 °C and 80 °C, in the 5%–80% RH range; these are presented in Section 3.1 and corroborated by simulation results in Section 3.2. The following Sections 3.3 and 3.4 show how the isotherms are impacted by increasing the maximum RH above 80%, and decreasing it below 5%. The effect of changing drying/wetting rate (through the stabilization threshold ε) and the differences from first to second isotherm loops are addressed in Section 3.5. Finally, Section 3.6 discusses the impact of the reference mass used to normalize the water content in the DVS experiments.

3.1. Isotherms from 20 °C to 80 °C

Fig. 6 shows the impact of moderately high temperatures on the DVS isotherms of our samples. The results confirm the DVS data from Wu et al. [32], in Fig. 3, extending them below 25 °C and above 40 °C, showing in particular that:

- All the adsorption curves at different temperatures are similar to each other, and also to those in Fig. 3; small differences at the various temperatures are within the variation in results from using different samples or analyzers: *cf.* Fig. 5. The results are also qualitatively and quantitatively consistent with adsorption isotherms obtained using desiccators on similar pastes, *e.g.* in Fig. 2. This supports the interpretation that adsorption is near equilibrium;

- In the desorption branches, the main difference brought by higher temperatures is an increase in cavitation pressure, *viz.* the RH at which the isotherm sharply drops (around 40%–50% depending on the temperature). Such change is substantive and clearly greater than the variations between similar tests on different analyzers in Fig. 5. A smaller hysteresis at low RH is noticeable too. The previous DVS results from Wu et al. in Fig. 3, showed a similar trend of cavitation pressure and hysteresis, although to a lesser extent due the limited range of temperatures explored there (25 to 40 °C). Our results indicate that the shift in cavitation pressure and reduction in hysteresis increase further when raising the temperature to 80 °C;

- The results shown in Fig. 6, as well as those from Wu et al. [32], disagree with sorption experiments carried out using desiccators, which showed significant changes in the desorption isotherm and reduced hysteresis at all relative humidities, already at 70 °C (see Fig. 2). However, the results from desiccators in Fig. 2 were for first desorption, which entails large irreversible changes in microstructure, whereas the DVS results in Fig. 6 are for second cycles. Also, the DVS experiments enable a more precise control of humidity and temperature and a smaller timescale for mass stabilization after changes in RH, all of which favor the observation of a more stable and consistent desorption branch. Further dedicated work would be required to investigate in more detail the relationship between results from DVS and from desiccators.

A clear difference between our results and those of Wu et al. [32] in Fig. 3, is that our results in Fig. 6 show significantly less hysteresis. This difference, however, is simply due to our isotherms being limited to the 5%–80% humidity range, as opposed to the 0%–95% RH range in Fig. 3.

3.2. DFT simulations

Fig. 7 shows results of DFT simulations of water sorption isotherms for a dense packing of particles representing the gel product in a cement paste at w/c = 0.4. The snapshots at different RH during adsorption and desorption, in Fig. 7.a, highlight two key mechanisms: the ink-bottle effect and cavitation. These are best appreciated starting from near
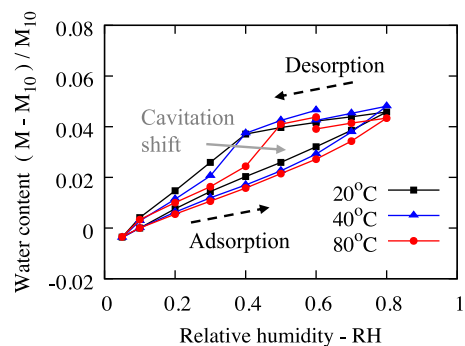

Fig. 6. Second-cycle DVS isotherms of our sample (CEM I paste, w/c = 0.4) at different temperatures, in the 5%–80% RH range. For the samples at 20 and 40 °C the stabilization threshold is $\varepsilon = 10^{-6}$ min^{-1}; for the sample at 80 °C, $\varepsilon = 10^{-5}$ min^{-1}. The solid arrow highlights the increase of cavitation pressure. The dashed arrows help identify the adsorption and desorption branches.

saturation, at RH 99%, where all the pores are filled with water. The snapshots at just lower RH = 80% indicate that the amount of water in the gel pores is much larger during desorption than during adsorption: this is due to the ink-bottle effect, whereby larger pores surrounded by smaller ones can develop a capillary meniscus and thus release their water only after the smaller pores around them are emptied. This entails that the actual humidity to empty the larger pores is lower than the equilibrium humidity to fill them up, producing hysteresis in the sorption isotherm. The snapshots at 60% RH in Fig. 7.a, instead, show a similar content and distribution of water during adsorption and desorption. This is due to the mechanism of cavitation, *i.e.* the liquid water in the gel pores reaching equilibrium with its vapor phase and therefore evaporating without relying on the formation of a capillary meniscus. As a result, evaporation also becomes independent of pore size and the ink-bottle effect is overridden.[3]

The isotherms computed at various temperatures, between 20 °C and 70 °C, are shown in Fig. 7.b. The adsorption isotherms from the simulations are qualitatively and quantitatively similar to the experimental ones. Their weak dependence on temperature supports the interpretation that adsorption is near equilibrium. The simulated desorption branches in Fig. 7.b predict one of the main effects that we observed experimentally, *viz.* that higher temperatures induce a shift towards higher cavitation pressures. The simulated cavitation pressures are systematically higher than the experimental ones, *e.g.* ~65% *vs.* the experimental ~40% at 20 °C. This overestimation is a known feature of the DFT method used in the simulations, already noted and discussed elsewhere [29,48]. The second experimental effect of higher temperatures, *viz.* the reduction of hysteresis at low RH, is not captured by the simulations. This is because hysteresis below the cavitation RH is governed by interlayer water in the calcium-silicate-hydrate phase: see *e.g.* Pinson et al. [5] for how different pore spaces contribute to sorption hysteresis in the cement paste. Indeed our experiments in Fig. 6, where desorption stops at 5% RH leaving much of the interlayer water unperturbed, feature significantly less hysteresis at low RH than experimental results where desorption continues down to 0% and interlayer water is mobilized, *e.g.* in Fig. 3 and later results in Section 3.4. In the DFT simulations, interlayer spaces are not resolved at all, therefore their contribution to sorption and hysteresis is completely missed.

The simulations provide a quantification and mechanistic explanation of the out-of-equilibrium nature of desorption at high RH. Fig. 7.c shows the evolution of the grand potential during a cycle of adsorption and desorption at various temperatures. As detailed in Section 2.3 in

---

[3] Actually, confinement at the water–solid interface does induce some pore size dependence, which becomes important in small pores and largely hinders cavitation in the interlayer spaces.
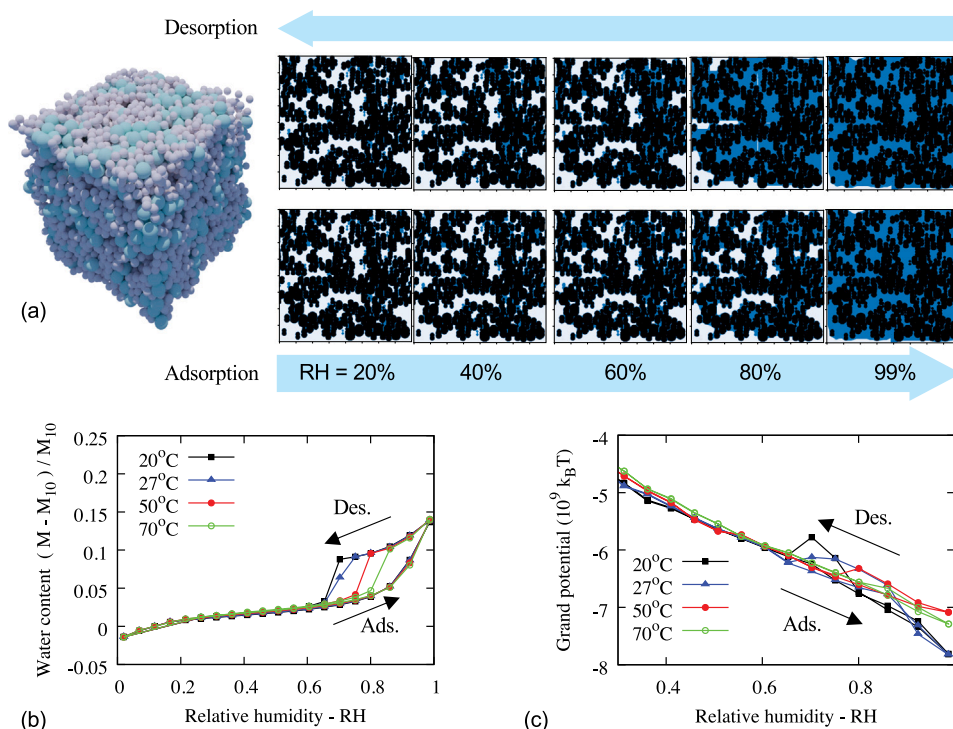
Fig. 7. DFT simulations of sorption isotherms: (a) dense configuration of particles, with solid fraction of *ca.* 0.64, representing the gel product in a cement paste, and cross section of the configuration at different humidities during adsorption and desorption at 20 °C; (b) water sorption isotherms simulated at different temperatures, with sample masses *M* computed assuming that the solid particles are made of C–S–H (more details in Refs. [29,48]); (c) evolution of the grand potential during adsorption and desorption.

the methodology, the grand potential represents the free energy to minimize. In Fig. 7.c, the grand potential at high humidity, *viz.* where hysteresis occurs in the simulations, is higher during desorption than during adsorption. This means that desorption is farther from equilibrium than adsorption. Fig. 7.a shows that the mechanism keeping desorption out of equilibrium is the ink-bottle effect. This effect creates pockets of condensed water that cannot evaporate until smaller pores surrounding them are emptied, which mainly occurs at cavitation in the small-size model system used here.[4] The impact of the ink-bottle effect can be appreciated by comparing the snapshots at 80% RH in Fig. 7.a during adsorption and desorption, the latter being clearly more saturated, whereas differences disappear at humidity below cavitation. These simulation results confirm that, in complex pore networks such as that of cement paste, the ink-bottle is the leading mechanism keeping the system out of equilibrium.

3.3. Effect of increasing the maximum RH from 80% to 98%

Fig. 8 shows how the DVS isotherms change upon increasing the maximum relative humidity explored in the cycles, RH_{max}, from 80% to 98%. Data for 80 °C was unavailable because the *DVS Resolution* analyzer could only achieve a maximum 80% RH when performing measurements at 80 °C. The isotherms in the figure are all second cycles, except for that at 40 °C reaching 98% RH, which is a first cycle because the data of the second cycle were lost. Section 3.5 will show that differences between first and second DVS cycles at 40 °C are marginal, both in the 5%–80% and in the 0%–98% ranges of humidity. Therefore we extrapolate that also the first cycle isotherm in the 5%–98% RH range is likely to be similar to a second cycle isotherm. Data for 20 °C consider two samples with significantly different initial masses,

---

[4] Large scale experiments feature a more gradual exhaustion of ink-bottles as the RH decreases during desorption, until a more abrupt disruption at cavitation causes the characteristic drop in saturation degree.
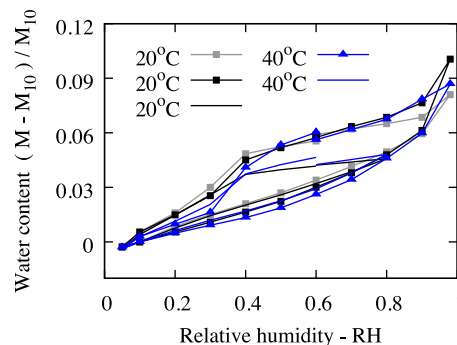

Fig. 8. DVS isotherms of our sample (CEM I paste, w/c = 0.4) at different temperatures, in the 5%–98% RH range (solid lines) and comparison with previous results from Fig. 6 in the 5%–80% RH range (dashed lines). All curves are second cycles, except for the dataset at 40 °C reaching 98% RH, which is a first cycle. In all cases, the stabilization threshold is $\varepsilon = 10^{-6}$ min^{-1}.

ca. 191 and 41 mg: see Table 2. The similar isotherms obtained for these two samples indicate that sample mass does not affect the results for the range of masses explored in this work.

The adsorption branches are not affected by the higher RH_{max}, and the trends between 80% and 98% RH are a convincing continuation of the results stopping at 80% RH. This also indicates that adsorption is at equilibrium, because if one used equilibrium-based models to extract microstructural information, *e.g.* the Kelvin equation, all adsorption branches in Fig. 8 would provide consistent results, irrespective of the maximum RH reached. This would not be true for the desorption branches. When stopping the cycle at 98% RH instead of 80% RH, the desorption branch features a higher saturation degree and also a steeper gradient, down to RH as low as the onset of cavitation, ~40%. The gradient, if interpreted using equilibrium-based microstructural models, would lead to the improbable conclusion that the microstructure changes significantly during a second cycle, depending on the
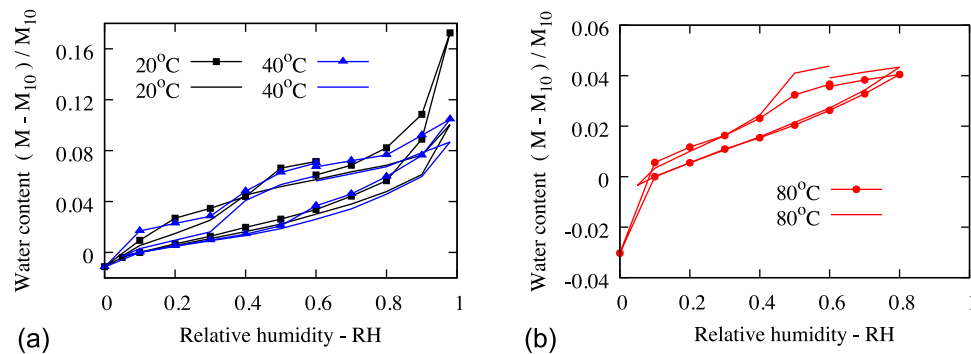
Fig. 9. DVS isotherms of our sample (CEM I paste, w/c = 0.4) at (a) 20 °C, 40 °C, and (b) 80 °C. Solid lines indicate 0%–98% RH range for samples at 20 °C and 40 °C, and 0%–80% RH range for the sample at 80 °C. Dashed lines stop at 5% minimum RH and correspond to data already shown in Fig. 8 for samples at 20 °C and 40 °C, and in Fig. 6 for the sample at 80 °C. All curves are second cycles, except for the dataset at 40 °C stopping at 5% minimum RH: see discussion on this point in relation to Fig. 8. The stabilization threshold for the tests reaching 0% RH is $\varepsilon = 10^{-6}$ min^{-1} for the samples at 20 °C and 40 °C, and $3 \cdot 10^{-7}$ min^{-1} for the sample at 80 °C.

maximum RH reached. On the other hand, the flatter desorption branch when stopping at 80% RH is consistent with the ink-bottle effect, without having to assume microstructural changes (see Ref. [5], where almost flat scanning loops during desorption were indeed predicted by modeling the ink-bottle effect). The larger hysteresis when reaching 98% RH, for humidities above cavitation, is also explained by the ink-bottle effect, which creates more pockets of condensed water maintaining higher saturation during desorption. Below cavitation, the ink-bottle effect is removed and, consistently, the desorption isotherms reaching 98% RH become very similar to those obtained by stopping at 80% RH. The isotherms at 40 °C display less hysteresis at low RH compared to the isotherms at 20 °C; this trend emerges from both the isotherms reaching 98% RH and those stopping at 80% and is probably linked to the mobilization of interlayer water.

3.4. Effect of decreasing the minimum RH from 5% to 0%

Fig. 9 shows the isotherms for which the minimum RH reached, RH$_{min}$, was 0% instead of 5%. At all temperatures, significant desorption takes place below 5% RH. This is expected because a large fraction (25%–50%) of the interlayer water in the calcium–silicate–hydrate phase only evaporates below 5% RH [49]. A less predictable result in Fig. 9 is that the extent of desorption below 5% is quantitatively similar at all temperatures. At 20 and 40 °C, this result matches previous DVS isotherms from Wu et al., in Fig. 3. Our result at 80 °C instead is novel and its comparison with literature data at similar temperatures, only available from larger-scale desiccator tests, is not straightforward due to inconsistencies in the literature itself. Indeed, the literature results in Fig. 1.b are quite similar to ours, whereas those in Fig. 1.a indicate that less and less desorption should occur below 5% RH as higher temperatures are sampled.

At 20 and 40 °C the adsorption isotherms feature higher saturation for the samples dried to 0% RH; this is especially evident at RH > 40%. This may be interpreted as the result of microstructural changes that may occur when drying down to 0% RH, but not when stopping at 5% RH. Another reason may be adsorption in C–S–H interlayer spaces that become desaturated when drying down to 0% RH, but not as much when stopping at 5% RH. Indeed, interlayer adsorption occurs with steep gradients at RH above 60% RH [5,7], in which region the differences between adsorption isotherms in Fig. 9 are greatest. Actually, the two interpretations are compatible, in that proton NMR experiments have shown that there is a conversion of gel pores and interlayer spaces during adsorption and desorption when reaching very low and very high humidities [31]. This means that mobilization of interlayer water is indeed linked to reversible nanostructural changes that may justify the differences in adsorption isotherms at high RH, depending on how low the RH is set during drying.

At 20 and 40 °C, the second-cycle desorption isotherms also changed when drying down to 0% RH instead of stopping at 5%. One evident difference, at RH > 80%, is the consequence of the higher adsorption at high RH, already discussed above. Between 80% RH and the cavitation threshold, RH ∼40%, the gradients of the desorption isotherms are similar for all the curves in Fig. 9.a. Instead at low RH, below cavitation, the desorption isotherms when RH$_{min}$ = 0% display a higher water content, and therefore a larger hysteresis, compared to the samples dried to 5% RH only. This can be explained as a combined effect of mobilization of interlayer water in the C–S–H and normalization to M_{10} employed in Fig. 9.a. Specifically, the reference interlayer water content (at RH = 10% during adsorption) is lower in samples dried to 0% RH than in those dried to 5% RH, because interlayer water is adsorbed progressively as the RH is increased from 0 to 100%. Instead, upon desorption, interlayer water is known to mostly evaporate at RH < 5%–10% [5].[5] As a result, the difference in water content during desorption and adsorption at low RH (i.e. the hysteresis there) is greater for samples dried to 0%.

At 80 °C, Fig. 9.b shows that the isotherms are very similar irrespective of whether the minimum RH$_{min}$ is 0 or 5%. A large desorption occurs below 5% RH, but an equally large adsorption takes takes place in the same range of low RHs. This indicates that moderately high temperatures are sufficient to drastically reduce the hysteresis associated with interlayer water, at least in the cases explored here, where the maximum RH at 80 °C is limited to 80%.

3.5. Effect of equilibration rate and differences between first and second cycles

Fig. 10 shows that first and second cycle isotherms are generally similar, irrespective of the equilibration rate used in the experiments (controlled by the stabilization threshold ε). A significant difference lies in the first desorption isotherms, starting at 60% RH, which differ from second-loop desorption curves for all the temperatures and rates explored. This result is the predictable consequence of microstructural changes during first desorption. Such changes are larger at higher temperature, as shown by the increasing difference between first and second desorption isotherms at 20, 40 and 80 °C in Fig. 10.a, and at 20 and 40 °C in Fig. 10.b. This trend is not an artifact of the normalization

---

[5] The hypothesis that interlayer water evaporates at very low RH and is adsorbed progressively across the full range of RH is a classical one, originally put forward by Feldman and Sereda [9]. In 2015, Pinson et al. [5] appreciated how recent results from proton NMR and atomistic simulations supported indeed the seminal hypothesis. This might be explained by that evaporation and adsorption of interlayer causing changes in the nanopore structure of the material; such changes were indeed detected using proton NMR, which also showed that they are reversible [31].
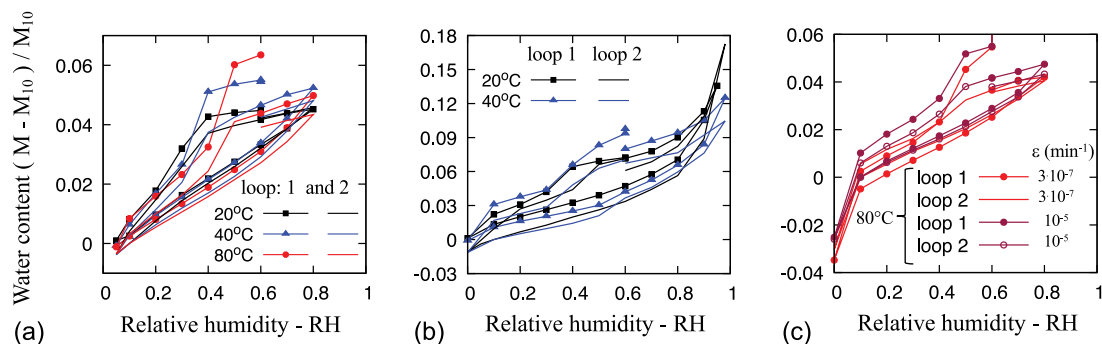
Fig. 10. Comparison of first and second cycle DVS isotherms of our sample (CEM I paste, w/c = 0.4): (a) samples at all temperatures tested at RH between 5% and 80%, with $\varepsilon = 10^{-5}$ min^{-1} and 10^{-6} min^{-1} respectively during the first and second loop (the latter already plotted in Fig. 6); (b) samples at 20 and 40 °C, tested between RH = 0% and 98%, with both loops at $\varepsilon = 10^{-6}$ min^{-1} (second loops already plotted in Fig. 9.a); (c) samples at 80 °C with two cycles at $\varepsilon = 3 \cdot 10^{-7}$ min^{-1} (same second loop as plotted in Fig. 9.b) and 10^{-5} min^{-1}. For all the curves, the water content of each sample is normalized by its mass M$_{10}$ at RH = 10% during second-cycle adsorption.
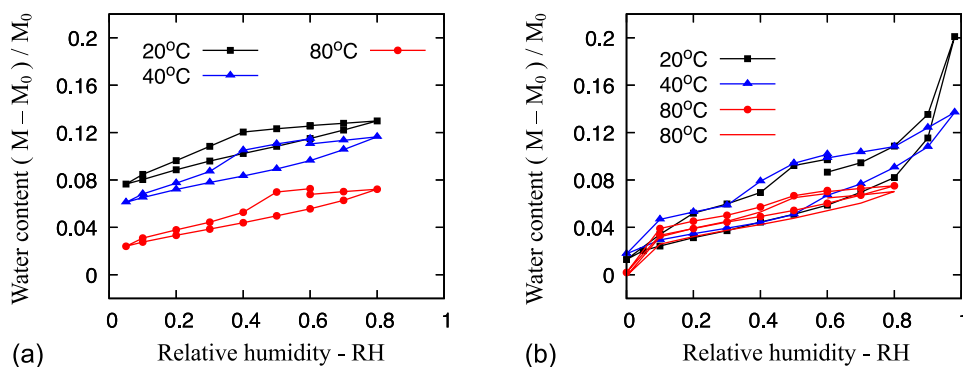

Fig. 11. Effect of normalizing water content by dry mass, after 24 h at 105 °C: (a) second cycles of adsorption and desorption between RH 5% and 80%, with $\varepsilon = 10^{-6}$ min^{-1} (same curves as in Fig. 6, but normalized by M_{10}); (b) second cycles of adsorption and desorption reaching minimum RH = 0%, with $\varepsilon = 10^{-6}$ min^{-1} for samples at 20 °C and 40 °C, and $\varepsilon = 10^{-5}$ min^{-1} (solid lines) and $3 \cdot 10^{-7}$ min^{-1} (dashed lines) for the samples at 80 °C.

of water content by M_{10}, as it would also emerge if the results were normalized by the dry mass M_0 of the samples; this other normalization is not displayed here, but the interested reader can reconstruct the isotherms using the M_0 values in Table 2.

3.6. Normalization by dry mass

In the literature on sorption experiments of cementitious materials, sample masses are usually normalized by dry mass. Such normalization is important, to perform meaningful comparisons between tests under different conditions. The results in this section show that normalization by dry mass is only effective when samples are tested at the same temperature, or when the minimum RH reached in the desorption branches is 0%. In all other cases, another state of the system that is consistent across the range of experimental conditions explored should be found.

Here we normalized the water content for the isotherms using sample masses at 10% RH during second adsorption, M_{10}, instead of dry mass after 24 h 105 °C, M_0. Fig. 11.a justifies this decision, in that isotherms with minimum RH = 5% become significantly shifted when the water content is normalized by M_0. This may confound the presentation of our results, as in multiple instances we have stopped desorption at 5% RH to sample evaporation and condensation in meso-pores while limiting the mobilization of interlayer water. However, despite the shift, all the isotherms in Fig. 11.a remain parallel, hence models using the gradient of these curves to compute pore size distributions would still return consistent results as discussed in this article when normalizing by M_{10}.

The shift in second-cycle isotherms in Fig. 11.a indicates that samples tested at higher temperature retain less water than samples tested at lower temperatures, throughout the entire range of relative humidity. On the other hand, Fig. 11.b shows that the shift disappears when the minimum RH reached is 0%; in this case, all the adsorption isotherms at different temperatures collapse onto the same curve, as expected. Also, the isotherms at 80 °C are very similar between Fig. 11.a and b, meaning that the impact of the minimum RH reached during the experiment becomes negligible at high temperatures. All these results in Fig. 11 suggest that higher temperatures favor evaporation of interlayer water already at relatively high RH, whereas at lower temperatures, such evaporation is only possible at very low RH, approaching 0%. As a result, normalization by M_0 (as usually adopted in the literature) only returns matching isotherms at different temperatures when a minimum RH of 0% is reached. When this is not the case, we recommend normalizing the water content by a suitably low RH during adsorption, e.g. M_{10} as proposed in this work.

3.7. Towards a model of sorption isotherms at moderately high temperatures

Based on our results, we propose here a conceptual framework to model sorption isotherms of cement pastes at moderately high temperatures. We start with the model in Pinson et al. [5], which split the isotherm into three contributions: one from water in interlayer spaces within the C–S–H, one from water adsorbed onto the surfaces of larger pores (gel and capillary), and one from condensed water in gel and capillary pores. For simplicity, hereafter we neglect the surface-adsorbed water whose contribution is usually quite small for typical pastes: see figure 4 in Pinson et al. [5].

Fig. 12 schematically reproduces the contributions to the sorption isotherm from interlayer and gel/capillary water, as proposed by
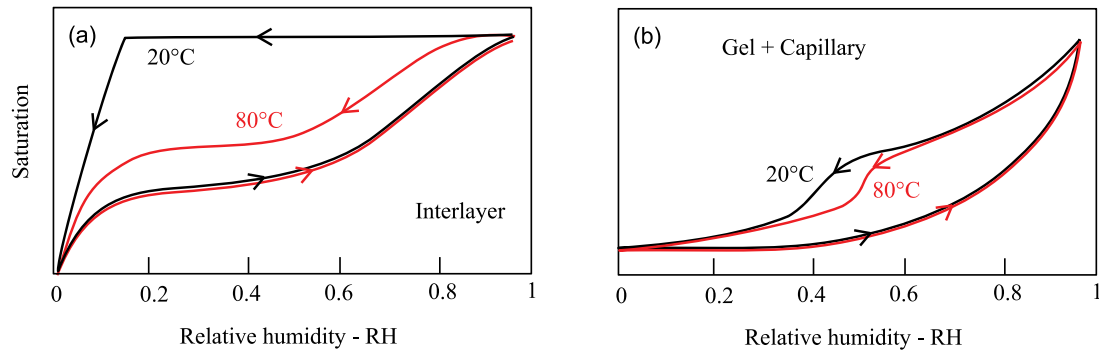
Fig. 12. Illustrations of contributions to the water sorption isotherm of a cement paste, from (a) water in the interlayer spaces of C–S–H, and (b) water in larger, gel and capillary, pores. The black curves, for room temperature, are inspired by those in Pinson et al. [5]. The red curves, at high temperature, are qualitatively proposed based on the results in this article. (For interpretation of the references to color in this figure legend, the reader is referred to the web version of this article.)

Pinson et al. for room temperature, 20 °C. In the same figure, we qualitatively outline the effect that a higher temperature may have on these contributions, according to the results in this article: we nominally associate this temperature to 80 °C. In particular, we propose that:

1. The adsorption branches are independent of temperature (neglecting the marginal effects that temperature has on the thermodynamic relationship between RH and size of the largest saturated capillary pore, *e.g.* the weak temperature-dependence of the Kelvin equation);
2. The only effect that temperature has on the isotherm from gel/capillary water, in Fig. 12.b, is a shift in the cavitation pressure, as per our DFT simulations. In Ref. [50], the interested reader can find a detailed study on temperature dependence of water cavitation from short-term sorption experiments on hardened cement pastes and other minerals;
3. The higher temperature, instead, significantly reduces the water content for the desorption branch of the isotherm from the interlayer water, in Fig. 12.a. This is already affecting the isotherm at relatively high RH.

Using the partial isotherms in Fig. 12, we can recover some of the qualitative experimental trends that have emerged in this article. Fig. 13.a and b show patterns of desorption and adsorption akin to our experiments in the 5%–80% humidity range. We start with the material at RH = 60%, assuming that the interlayer spaces are fully saturated irrespective of the temperature: see white dots in the figures. The first desorption takes the sample down to 5% RH and onto the respective desorption curve from Fig. 12, depending on the test temperature. Adsorption then brings the sample to 80% RH: for the contribution of the gel and capillary pores, both samples at 20 °C and 80 °C follow approximately the same adsorption curve,corresponding to that of samples fully dried to 0% RH in Fig. 12. On the contrary, the interlayer contribution depends considerably on the temperature. Namely, adsorption at 80 °C branch is very similar to that of a fully dried sample, as in Fig. 12, whereas at 20 °C, a large part of interlayer water is not evaporated and the adsorption branch remains flatter until reconciling with the near-equilibrium adsorption branch at higher RH. Desorption from 80% back to 5% then follows a straight line that closes the hysteresis loop for both samples at 20 and 80 °C. The result of this protocol, for the interlayer isotherm, is twofold: first, samples tested at lower temperature display more hysteresis, which is in line with our result in Fig. 6; second, if the isotherms are normalized by dry mass, as done in Fig. 11, the isotherm obtained at lower temperature will be shifted above the isotherm at higher temperature, as per our experimental result in Fig. 11.a.

Fig. 13.c and d show the contributions to sorption isotherms for tests in the 5%–98% humidity range. In this case, adsorption follows the same curves as for the 5%–80% protocol in Fig. 13.a and b. At 80 °C, desorption from 98% RH down towards 5% follows the same curve as in the 5%–80% protocol, just starting from a higher initial RH. By contrast, at 20 °C, desorption follows a horizontal line that keeps the interlayer spaces fully saturated until very low RH. As a result, the low-RH hysteresis at low temperature increases when a higher RH is reached during adsorption, whereas at higher temperature the low-RH hysteresis is less affected. This agrees qualitatively with our experimental results for temperatures of 20 °C and 40 °C in Fig. 8. Furthermore, Fig. 13.c and d show that for the 5%–98% RH protocol, isotherms obtained at lower temperature would sit above those at higher temperature, if both are normalized by the dry mass of the sample; although we did not display these results, our experiments confirm indeed the shift also for the 5%–98% RH protocol (the interested reader can reconstruct it from the results in Fig. 8 and the dry mass values in Table 2). According to the model isotherms in this section, the shift would disappear when reaching RH = 0% during drying, because in this case the isotherms in Fig. 12 would be recovered (even when reaching a maximum RH lower than 100%). This agrees with our experimental result in Fig. 11.b, where normalization by dry mass provides matching isotherms at all temperatures when drying is pushed down to 0% RH.

4. Conclusion

We presented new dynamic vapor sorption (DVS) data for a water–cement ratio 0.4 CEM I paste, at 20, 60, and 80 °C. The results confirmed and extended previous trends measured in a narrower range of temperatures, 25–40 °C. The key findings are:

- Adsorption is near-equilibrium, and desorption is not. Indeed, all the adsorption curves from various testing protocols and at different temperatures returned very consistent isotherms, whose interpretation through thermodynamic models, such as the Kelvin equation, would lead to very consistent pore size distributions. This implies that moderately high temperatures, like those sampled here, do not induce significant microstructural changes, at least in 1–100 nm range of length scales sampled by vapor sorption;
- The main effect that moderately high temperatures have on desorption is to increase the RH at which cavitation occurs. Dedicated DFT simulations predicted this effect as a result of the ink-bottle mechanisms, whereby higher temperatures destabilize the metastable capillary menisci in a model structure of gel pores in the cement paste. The simulation results confirmed that this process does not necessitate any microstructural change, and that
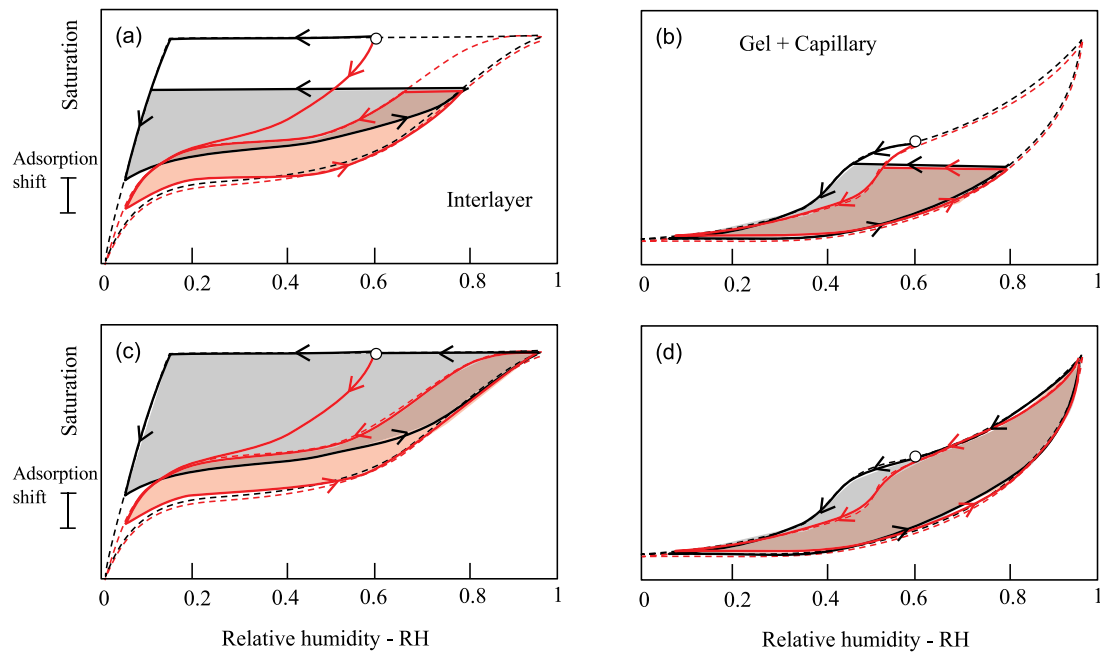
Fig. 13. Contributions to sorption isotherms from interlayer water and from water in gel and capillary pores: (a,b) testing protocol between RH = 5% and 80%; and (c,d) testing protocol between RH = 5% and 98%. The white dots are the starting points of the first desorption, at 60%, assuming full saturation of the interlayer pores at this point. The shaded areas help the reader appreciate the second-cycle hysteresis resulting from the different protocols.

a model system of C–S–H and adsorbed water has a higher free-energy, *i.e.* it is further away from equilibrium, during desorption than adsorption;

- The second effect of higher temperatures is a downward shift of the desorption isotherm, *viz.* a reduction of the saturation level at all RHs during desorption. This overall reduces the hysteresis at higher temperatures, since we already concluded that adsorption is not affected. Experiments evaluating isotherms in various ranges of RH (5%–80%, 5%–98%, and 0%–98%) indicated that the smaller hysteresis may reflect a smaller hysteresis associated to water in interlayer spaces, and in particular a greater tendency of interlayer water to evaporate at higher RH when samples are tested at higher temperatures.

A limitation of this study is that, due to the serial (hence relatively time-consuming) nature of the DVS experiments, we tested only one sample for each combination of RH range, temperature, and stabilization threshold. We still consider the results as significant, for three reasons: (i) previous literature results on the same cement paste as studied here, showed very little statistical variation in second cycle isotherms [32]; (ii) all our results showed very good consistency, both qualitative and quantitative, after rationalizing the effects of the various testing conditions as per our proposed model; (iii) we found that the stabilization threshold we explored here did not affect the isotherms; therefore, for each combination of RH range and temperature, the two/three samples tested imposing different thresholds may be considered, effectively, as equivalent.

The experimental results inspired a conceptual model for water sorption in cement pastes at moderately high temperatures. The model considers how two classes of pores contribute to the sorption process: interlayer spaces and larger pores (gel + capillary). The sorption curves for the larger pores capture the shift in condensation pressure due to the ink-bottle effect, whereas the interlayer isotherms feature the reduction in hysteresis at higher temperatures. The proposed model is simplified; for example, it assumes that the maximum water content in interlayer spaces does not depend on temperatures and that any temperature-induced changes in the interlayer structure are reversible. These aspects

would require further investigation. However, the proposed model already captures the main trends that emerged from the experiments, and it also explains why normalization of adsorbed mass by dry mass returns consistent isotherms at different temperatures only when the testing protocol involves drying down to 0% RH.

In this work we have considered only one cement mix based on CEMI, with water–cement ratio of 0.4, and aged for 28 days. Our results should apply directly also to CEMI mortars and concrete, as their sub-microstructure (sampled by DVS) should not change significantly, and these systems have relevance for many existing structures. However, mortars and concretes would often feature water-to-cement ratios other than 0.4; this aspect would deserve dedicated experiments. A further extension of our study would be to assess binders that are more techno-logically relevant; a first choice would be cements with supplementary cementitious materials (SCCs, *e.g.* fly ash and slags), which might significantly differ at the sub-micrometre scale. Further yet, one could test samples that have been cured for longer, for example 6 months, before starting the DVS experiments. For the mix in this work, longer curing should not produce major differences, except possibly reducing the extent of irreversible microstructural changes during first drying. A longer curing should however be considered for slower-hydrating mixes, such as various binders that incorporate SCCs. Irrespective of the binder type and its curing age, the work in this article is valuable in that it details an experimental approach that can be applied across cement systems, highlighting which testing conditions are likely or unlikely to impact the results. Also, our proposed model identified mechanisms that are likely to underpin the interpretation of analogous isotherms for other mixes, *e.g.* the role of interlayer and gel pores in higher-aluminium pastes where C–A–S–H takes over C–S–H as the main binding phase. All in all, the results in this article and the proposed model offer a starting point to develop improved constitutive laws for temperature-dependent water sorption in cement pastes.

Declaration of competing interest

The authors declare the following financial interests/personal relationships which may be considered as potential competing interests:

Marcus Yio, Hong Wong reports financial support was provided by Engineering and Physical Sciences Research Council.

Data availability

Data will be made available on request.

Acknowledgments

References

[1] M. Pathirage, D.P. Bentz, G. Di Luzio, E. Masoero, G. Cusatis, The ONIX model: a parameter-free multiscale framework for the prediction of self-desiccation in concrete, Cem. Concr. Compos. 103 (2019) 36–48.

[2] C.T. Davie, C.J. Pearce, K. Kukla, N. Bićanić, Modelling of transport processes in concrete exposed to elevated temperatures–An alternative formulation for sorption isotherms, Cem. Concr. Res. 106 (2018) 144–154.

[3] D. Gawin, F. Pesavento, B.A. Schrefler, Hygro-thermo-chemo-mechanical modelling of concrete at early ages and beyond. Part II: shrinkage and creep of concrete, Internat. J. Numer. Methods Engrg. 67 (3) (2006) 332–363.

[4] S. Rahimi-Aghdam, E. Masoero, M. Rasoolinejad, Z.P. Bažant, Century-long expansion of hydrating cement counteracting concrete shrinkage due to humidity drop from selfdesiccation or external drying, Mater. Struct. 52 (1) (2019) 1–21.

[5] M.B. Pinson, E. Masoero, P.A. Bonnaud, H. Manzano, Q. Ji, S. Yip, J.J. Thomas, M.Z. Bazant, K.J. Van Vliet, H.M. Jennings, Hysteresis from multiscale porosity: modeling water sorption and shrinkage in cement paste, Phys. Rev. A 3 (6) (2015) 064009.

[6] H. Ranaivomanana, J. Verdier, A. Sellier, X. Bourbon, Toward a better comprehension and modeling of hysteresis cycles in the water sorption–desorption process for cement based materials, Cem. Concr. Res. 41 (8) (2011) 817–827.

[7] E. Masoero, G. Cusatis, G. Di Luzio, C–S–H gel densification: The impact of the nanoscale on self-desiccation and sorption isotherms, Cem. Concr. Res. 109 (2018) 103–119.

[8] S. Poyet, S. Charles, Temperature dependence of the sorption isotherms of cement-based materials: Heat of sorption and Clausius–Clapeyron formula, Cem. Concr. Res. 39 (11) (2009) 1060–1067.

[9] R.F. Feldman, P.J. Sereda, A model for hydrated portland cement paste as deduced from sorption-length change and mechanical properties, Matér. Constr. 1 (6) (1968) 509–520.

[10] I. Maruyama, Y. Nishioka, G. Igarashi, K. Matsui, Microstructural and bulk property changes in hardened cement paste during the first drying process, Cem. Concr. Res. 58 (2014) 20–34.

[11] A.M. Gajewicz, E. Gartner, K. Kang, P.J. McDonald, V. Yermakou, A 1H NMR relaxometry investigation of gel-pore drying shrinkage in cement pastes, Cem. Concr. Res. 86 (2016) 12–19.

[12] T. Ishida, K. Maekawa, T. Kishi, Enhanced modeling of moisture equilibrium and transport in cementitious materials under arbitrary temperature and relative humidity history, Cem. Concr. Res. 37 (4) (2007) 565–578.

[13] F. Brue, C.A. Davy, F. Skoczylas, N. Burlion, X. Bourbon, Effect of temperature on the water retention properties of two high performance concretes, Cem. Concr. Res. 42 (2) (2012) 384–396.

[14] E. Drouet, S. Poyet, J.-M. Torrenti, Temperature influence on water transport in hardened cement pastes, Cem. Concr. Res. 76 (2015) 37–50.

[15] M. Ben Abdelhamid, D. Mihoubi, J. Sghaier, A. Bellagi, Water sorption isotherms and thermodynamic characteristics of hardened cement paste and mortar, Transp. Porous Media 113 (2) (2016) 283–301.

[16] J. Hundt, H. Kantelberg, Sorptionsuntersuchungen an zemestein, zementmörtel und beton (in German), CDeutscher Aussch. Stahlbeton Heft 297 (1978) 25–39.

[17] S. Poyet, Experimental investigation of the effect of temperature on the first desorption isotherm of concrete, Cem. Concr. Res. 39 (11) (2009) 1052–1059.

[18] Z.P. Bažant, W. Thonguthai, Pore pressure and drying of concrete at high temperature, J. Eng. Mech. Div. 104 (5) (1978) 1059–1079.

[19] Z.P. Bažant, W. Thonguthai, Pore pressure in heated concrete walls: theoretical prediction, Mag. Concr. Res. 31 (107) (1979) 67–76.

[20] F. Pesavento, Nonlinear Modelling of Concrete as Multiphase Porous Material in High Temperature Conditions (Ph.D. thesis), University of Padova, 2000.

[21] S. Poyet, Describing the influence of temperature on water retention using van genuchten equation, Cem. Concr. Res. 84 (2016) 41–47.

[22] T. Hozjan, M. Saje, S. Srpčič, I. Planinc, Fire analysis of steel–concrete composite beam with interlayer slip, Comput. Struct. 89 (1–2) (2011) 189–200.

[23] R.K.K. Yuen, W.K. Kwok, S.M. Lo, J. Liang, Heat and mass transfer in concrete at elevated temperature, Numer. Heat Transf. A: Appl. 51 (5) (2007) 469–494.

[24] D. Dauti, S. Dal Pont, B. Weber, M. Briffaut, N. Toropovs, M. Wyrzykowski, G. Sciumé, Modeling concrete exposed to high temperature: Impact of dehydration and retention curves on moisture migration, Int. J. Numer. Anal. Methods Geomech. 42 (13) (2018) 1516–1530.

[25] C.T. Davie, C.J. Pearce, N. Bićanić, A fully generalised, coupled, multi-phase, hygro-thermo-mechanical model for concrete, Mater. Struct. 43 (1) (2010) 13–33.

[26] Z. Wu, H.S. Wong, N.R. Buenfeld, Transport properties of concrete after drying-wetting regimes to elucidate the effects of moisture content, hysteresis and microcracking, Cem. Concr. Res. 98 (2017) 136–154.

[27] M.H.N. Yio, M.J. Mac, Y.X. Yeow, H.S. Wong, N.R. Buenfeld, Effect of autogenous shrinkage on microcracking and mass transport properties of concrete containing supplementary cementitious materials, Cem. Concr. Res. 150 (2021) 106611.

[28] J.-F. Daian, Condensation and isothermal water transfer in cement mortar part I—Pore size distribution, equilibrium water condensation and imbibition, Transp. Porous Media 3 (6) (1988) 563–589.

[29] T. Zhou, K. Ioannidou, E. Masoero, M. Mirzadeh, R.J.-M. Pellenq, M.Z. Bazant, Capillary stress and structural relaxation in moist granular materials, Langmuir 35 (12) (2019) 4397–4402.

[30] B. Bary, A polydispersed particle system representation of the porosity for non-saturated cementitious materials, Cem. Concr. Res. 36 (11) (2006) 2061–2073.

[31] M. Wyrzykowski, P.J. McDonald, K.L. Scrivener, P. Lura, Water redistribution within the microstructure of cementitious materials due to temperature changes studied with 1H NMR, J. Phys. Chem. C 121 (50) (2017) 27950–27962.

[32] M. Wu, B. Johannesson, M. Geiker, A study of the water vapor sorption isotherms of hardened cement pastes: Possible pore structure changes at low relative humidity and the impact of temperature on isotherms, Cem. Concr. Res. 56 (2014) 97–105.

[33] D.S. Carr, B.L. Harris, Solutions for maintaining constant relative humidity, Ind. Eng. Chem. 41 (9) (1949) 2014–2015.

[34] L. Greenspan, Humidity fixed points of binary saturated aqueous solutions, J. Res. Natl. Bureau Stand. A Phys. Chem. 81 (1) (1977) 89.

[35] J.F. Young, Humidity control in the laboratory using salt solutions—a review, J. Appl. Chem. 17 (9) (1967) 241–245.

[36] R.J. Flatt, G.W. Scherer, J.W. Bullard, Why alite stops hydrating below 80% relative humidity, Cem. Concr. Res. 41 (9) (2011) 987–992.

[37] V. Baroghel-Bouny, Water vapour sorption experiments on hardened cementitious materials: part I: essential tool for analysis of hygral behaviour and its relation to pore structure, Cem. Concr. Res. 37 (3) (2007) 414–437.

[38] E.L. Perkins, J.P. Lowe, K.J. Edler, N. Tanko, S.P. Rigby, Determination of the percolation properties and pore connectivity for mesoporous solids using NMR cryodiffusometry, Chem. Eng. Sci. 63 (7) (2008) 1929–1940.

[39] H. Garbalińska, M. Bochenek, W. Malorny, J. von Werder, Comparative analysis of the dynamic vapor sorption (DVS) technique and the traditional method for sorption isotherms determination—Exemplified at autoclaved aerated concrete samples of four density classes, Cem. Concr. Res. 91 (2017) 97–105.

[40] E. Gruyaert, C. Dieleman, N. De Belie, Influence of sample preparation and the addition of BFS on water vapour sorption isotherms, in: 12th International Conference on Durability of Building Materials and Components (XII DBMC-2011), Vol. 3, FEUP, 2011, pp. 1487–1494.

[41] P.A. Bonnaud, Q. Ji, B. Coasne, R.J.-M. Pellenq, K. Van Vliet, Thermodynamics of water confined in porous calcium-silicate-hydrates, Langmuir 28 (31) (2012) 11422–11432.

[42] P.A. Bonnaud, Q. Ji, K.J. Van Vliet, Effects of elevated temperature on the structure and properties of calcium–silicate–hydrate gels: the role of confined water, Soft Matter 9 (28) (2013) 6418–6429.

[43] A.C.A. Muller, K.L. Scrivener, A.M. Gajewicz, P.J. McDonald, Use of bench-top NMR to measure the density, composition and desorption isotherm of c—S—H in cement paste, Microporous Mesoporous Mater. 178 (0) (2013) 99–103.

[44] E. Masoero, E. Del Gado, R.J.-M. Pellenq, F.-J. Ulm, S. Yip, Nanostructure and nanomechanics of cement: Polydisperse colloidal packing, Phys. Rev. Lett. 109 (15) (2012) 155503.

[45] E. Masoero, H.M. Jennings, F.J. Ulm, E. Del Gado, H. Manzano, R.J.M. Pellenq, S. Yip, Modelling cement at fundamental scales: From atoms to engineering strength and durability, Comput. Model. Concr. Struct 1 (2014) 139–148.

[46] E. Kierlik, P.A. Monson, M.L. Rosinberg, L. Sarkisov, G. Tarjus, Capillary condensation in disordered porous materials: Hysteresis versus equilibrium behavior, Phys. Rev. Lett. 87 (5) (2001) 055701.

[47] E. Kierlik, P.A. Monson, M.L. Rosinberg, G. Tarjus, Adsorption hysteresis and capillary condensation in disordered porous solids: a density functional study, J. Phys.: Condens. Matter 14 (40) (2002) 9295.

[48] T. Zhou, K. Ioannidou, F.-J. Ulm, M.Z. Bazant, R.J.-M. Pellenq, Multiscale poromechanics of wet cement paste, Proc. Natl. Acad. Sci. 116 (22) (2019) 10652–10657.

[49] M.B. Pinson, T. Zhou, H.M. Jennings, M.Z. Bazant, Inferring pore connectivity from sorption hysteresis in multiscale porous media, J. Colloid Interface Sci. 532 (2018) 118–127.

[50] I. Maruyama, J. Rymeš, M. Vandamme, B. Coasne, Cavitation of water in hardened cement paste under short-term desorption measurements, Mater. Struct. 51 (6) (2018) 1–13.